



Dayside magnetopause reconnection and flux transfer events: BepiColombo earth-Flyby observations

Weijie Sun¹, James A. Slavin¹, Rumi Nakamura², Daniel Heyner³, Karlheinz J. Trattner⁴, Johannes Z. D. Mieth³, Jiutong Zhao⁵, Qiu-Gang Zong⁵, Sae Aizawa^{6,7}, Nicolas Andre⁶, Yoshifumi Saito⁸

- 5 ¹Department of Climate and Space Sciences and Engineering, University of Michigan, Ann Arbor, MI 48109, United States
²Space Research Institute, Austrian Academy of Sciences, Schmiedlstraße 6, 8042 Graz, Austria
³Institut für Geophysik und extraterrestrische Physik, Technische Universität Braunschweig, 38106 Braunschweig, Germany
10 ⁴Laboratory for Atmospheric and Space Physics, University of Colorado, Boulder, CO 80303, USA
⁵School of Earth and Space Sciences, Peking University, Beijing 100871, China
⁶Institut de Recherche en Astrophysique et Planétologie, CNRS-UPS-CNES, Toulouse, France
⁷Department of Geophysics, Graduate School of Science, Tohoku University, Sendai, Japan
⁸Japan Aerospace Exploration Agency, Institute of Space and Astronautical Science, Kanagawa, Japan
15 *Correspondence to:* Weijie Sun (wjsun@umich.edu)

Abstract. This study analyzes the flux transfer event (FTE)-type flux ropes and magnetic reconnection around the dayside magnetopause during BepiColombo's Earth flyby. The magnetosheath corresponds to a high plasma β (~ 8) and the IMF has a significant radial component. Six flux ropes are identified. The motion of flux rope together with the maximum magnetic shear model suggests that the reconnection X-line swipes BepiColombo near the magnetic equator due to an increase of the radial IMF. The flux rope with the highest flux content contains a clear coalescence signature, i.e., two smaller flux ropes merging, supporting theoretical predictions the flux content of flux ropes can grow through coalescence. The secondary reconnection associated with coalescence exhibits a large normalized guide field and a reconnection rate comparable to the reconnection rate measured at the magnetopause (~ 0.1).

1. Introduction

25 Flux transfer events (FTEs) are frequently observed near the outer boundaries of planetary magnetospheres, including at the Earth (e.g., Russell and Elphic, 1978; Saunders et al., 1984; Wang et al., 2005), Mercury (Russell and Walker, 1985; Slavin et al., 2009; 2010; 2012; Imber et al., 2014; Sun et al., 2020), Saturn (Jasinski et al., 2016; 2021) and Jupiter (Walker and Russell, 1985; Lai et al., 2012). Some of the FTEs have magnetic flux ropes at their cores, which consist of helical magnetic field lines surrounding stronger magnetic fields paralleling their central axes (Paschmann et al., 1982; Lee et al., 1993). These FTE-type flux ropes are created by multiple X-line reconnections in the magnetopause during intervals of significant magnetic shear across this current sheet (Lee and Fu, 1985; Raeder, 2006). As a result, the FTE-type flux ropes signal not only the occurrence of magnetic reconnection but their direction of travel can be used to infer the relative location of the reconnection X-lines at the magnetopause.



35 FTEs contribute to the transport of magnetic flux from the dayside to the nightside magnetosphere that drives the
Dungey cycle in dipolar planetary magnetospheres. In Mercury's magnetosphere, the FTE-type flux ropes transport
majority of (>60%) the circulated flux (Slavin et al., 2010; Imber et al., 2014; Sun et al., 2020). In contrast, FTE-
type flux ropes are estimated to transport only a small portion (<5%) of the circulated flux at Earth (Lockwood et al.,
1995; Fear et al., 2017). And for the giant outer planetary magnetospheres at Jupiter and Saturn, they appear to
40 transport a negligible magnetic flux (< 1%) for the solar wind-driven portion of their internal convection (Jasinski et
al., 2021).

FTEs at Earth are most frequent during periods of the southward interplanetary magnetic field (IMF) when the
magnetic shear angle across the magnetopause is larger than 90° (e.g., Rijnbeek et al., 1984; Kuo et al., 1995; Wang
et al., 2006). The locations of magnetopause X-lines are closely related to the orientation of the IMF. For example,
45 during the purely southward IMF, reconnections most likely occur on the magnetopause near the subsolar point
(Dungey, 1961). During the purely northward IMF, reconnections occur on the magnetopause tailward of the cusp
(Dungey, 1961; Song and Russell, 1992; Shi et al., 2009; 2013). Magnetic reconnection is also thought to occur at
the dayside magnetopause under the strong radial IMF (B_x dominate) (Belenkaya, 1998; Luhmann et al., 1984; Pi et
al., 2017; Tang et al., 2013), but the strong radial IMF conditions are less well studied.

50 Coalescence events, which refer to the merging of neighboring flux ropes, are thought to be an important process in
space plasma physics (Biskamp and Welter, 1980; Dorelli and Bhattacharjee, 2009; Fermo et al., 2011; Hoilijoki et
al., 2017). The merging of flux ropes is associated with secondary reconnection, and changes in magnetic field
configuration caused by this secondary reconnection can energize particles, especially electrons (Drake et al., 2006).
Furthermore, several studies have suggested that FTE-type flux ropes are initially formed at electron to ion scales.

55 They then grow through coalescence, thereby, increasing their magnetic flux content (Fermo et al., 2011; Akhavan-
Tafti et al., 2018). NASA's Magnetospheric Multiscale (MMS) Mission (Burch et al., 2016) has provided several
observations between neighboring flux ropes, for example, Øieroset et al. (2016); Zhou et al. (2017); and Kacem et
al. (2018).

This study investigates FTE-type flux ropes and reconnection at the Earth's dayside magnetopause during
60 BepiColombo's flyby on 10 April 2020. The paper is arranged as follows. Section 2 introduces the BepiColombo
mission and the measurements during the dayside magnetopause crossing. Section 3 analyzes the distribution of
magnetopause reconnection with a strong radial IMF component, and the properties of the flux ropes, including a
coalescence event. Section 4 provides a summary of our results.

2. BepiColombo Dayside Magnetopause Crossing

65 2.1. Spacecraft and Instrumentation

BepiColombo, which is a joint mission by the ESA and the JAXA, consists of two spacecraft, which are the
Mercury Planetary Orbiter (MPO) and Mercury Magnetospheric Orbiter (MMO, or Mio). These spacecraft together
will carry out detailed investigations of Mercury's interior, surface, exosphere, and magnetosphere (Milillo et al.,
2020; Murakami et al., 2020; Benkhoff et al., 2010). The mission made its first planetary flyby maneuver at Earth on
70 10 April 2020 (Mangano et al., 2021), during which several instruments collected measurements.



75

This study uses measurements collected by the magnetometer (MAG) onboard MPO (Heyner et al., 2021), the low energy electron by Mercury Electron Analyzer (MEA) (Sauvaud et al., 2010), which is part of the Mercury Plasma Particle Experiment (MPPE) onboard Mio (Saito et al., 2021). The MPO/MAG includes one outbound sensor and one inbound sensor, and it has a sampling rate of 128 Hz. Mio/MEA has a sampling rate of 4 s. The IMF and solar wind conditions are obtained from the OMNI dataset (King and Papitashvili, 2005), which has a time resolution of 1 minute.

2.2. Overview of Magnetosheath and Magnetopause

80

Figure 1 shows an overview of the dayside magnetopause crossing during BepiColombo's Earth flyby. BepiColombo traveled from the magnetosheath into the dayside magnetosphere. It crossed the magnetopause at a distance of $\sim 4.8 R_E$ dawnward from the subsolar magnetopause. During the 30 minutes interval around the magnetopause crossing ($\sim 00:05$ to $00:35$ UT) analyzed here, the IMF was southward with a strong radial component. The B_x was the dominant component ($B_x/B_t > 0.7$ in Figure 1f). The average electron density in the magnetosheath was estimated to be $\sim 10 \text{ cm}^{-3}$ based on the onboard-calculated partial moment from Mio/MEA between $00:05$ and $00:28$. The magnetosheath plasma β was high with a value of ~ 8.0 , which was the ratio of the thermal pressure to the magnetic pressure. The thermal pressure in the magnetosheath was calculated by assuming that the pressure balance existed across the dayside magnetopause and that the thermal pressure inside the dayside magnetosphere was negligible compared to the magnetic pressure.

85

3. Magnetopause Reconnections and FTE-type Flux Ropes

3.1. Identification of FTE-type Flux Ropes

90

The FTEs were identified after the measured magnetic field was rotated into boundary normal coordinates (the LMN coordinates). The minimum variance analysis (MVA) (Sonnerup and Cahill Jr., 1967; Sonnerup and Scheible, 1998) was performed on the magnetic field measurements across the magnetopause current sheet from $00:32:30$ to $00:33:25$ UT. The MVA results produced $L = [0.10, 0.24, 0.97]$ (maximum variance direction), $M = [0.12, 0.96, -0.25]$ (intermediate variance direction), $N = [0.99, -0.14, -0.06]$ (minimum variance direction), and the eigenvalue ratios $\lambda_{max}/\lambda_{int} \sim 54.3$, $\lambda_{int}/\lambda_{min} \sim 3.9$. Both of the ratios were larger than 3 indicating that the LMN coordinate of the magnetopause was well determined [Sonnerup & Scheible, 1998].

95

The FTEs are identified with bipolar signatures in the normal magnetic field (B_N) and clear magnetic field rotation (Russell and Elphic, 1978). The identification of FTEs with flux rope cores requires the additional signature of a strong magnetic field along their central axis, i.e. the intermediate variance direction [e.g. Akhavan-Tafti et al., 2018]. Six FTE-type flux ropes were identified in this manner in the magnetosheath just upstream of the dayside magnetopause and marked with green arrows in Figure 1e and listed in Table 1.

100

The first FTE-type flux rope was observed at $\sim 00:11:03$ UT when the IMF clock angle was $\sim 210^\circ$, and $B_x/B_t \sim 0.75$. This flux rope traveled southward as inferred from the polarities of the B_N variation. About 2 minutes later, the clock angle increased to $\sim 260^\circ$. This IMF orientation persisted for about 12 minutes, during which no FTE-type flux ropes were observed. At $\sim 00:26:06$ UT, the clock angle decreased from $\sim 260^\circ$ to $\sim 210^\circ$ while the ratio of B_x/B_t

105



increased to ~ 0.90 . At this point, 5 FTE-type flux ropes successively appeared up to the point where the magnetopause was crossed. The direction of travel for these 5 flux ropes was inferred to be northward, again based on the B_N variations. The first flux rope traveled southward indicating that the primary magnetopause X-line was initially located northward of the spacecraft. Later, the northward motion of the 5 flux ropes indicated that the
110 primary magnetopause X-line(s) had shifted southward.

3.2. Reconnection X-lines from Maximum Magnetic Shear Model

To further investigate reconnection during BepiColombo's dayside magnetopause traversal, the maximum magnetic shear model (Trattner et al., 2007; 2017) was employed to deduce the location of the reconnection X-lines. The magnetic shear angle plots during the intervals centered at 00:09, 00:20, 00:28 UT are shown in Figure 2. Figures 2a
115 and 2b correspond to a distorted feature of the anti-parallel reconnection region, which has recently been termed a "Knee" event (Trattner et al., 2021). The bent shape of the anti-parallel reconnection region is associated with the field line draping in the magnetosheath during the dominant B_x (significantly sunward) component during this period.

In Figure 2a, BepiColombo was located southward of the predicted X-line. From Figure 2a to Figure 2b, the
120 predicted X-line crossed the location of BepiColombo and was then located to the south of BepiColombo. The changes of X-line locations from Figures 2a to 2b are due to the IMF clock angle decreased around 10° together with the B_x/B_i increased from 0.78 to 0.86.

The direction of motion for our FTE-type flux ropes was consistent with the predicted location of the reconnection X-line predicted by the maximum magnetic shear model during the changing solar wind conditions for this
125 magnetopause encounter. Figure 2a corresponded to the only southward traveling FTE-type flux rope, while the other five northward traveling FTE-type flux ropes were observed during the conditions shown in Figures 2b and 2c. Although the maximum magnetic shear model faces challenges in determining the draping magnetic field lines in the magnetosheath during the intervals of the dominant B_x component (Trattner et al., 2007; 2012), the model predictions were consistent with our observations during BepiColombo's crossing.

3.3. FTE-type Flux Rope Modeling

This study employs a force-free flux rope model (Kivelson and Khurana, 1995) to fit the FTE-type flux ropes. This flux rope model starts from the periodic pinch solution (Schindler et al., 1973) of Ampere's law ($\nabla \times \vec{B} = \mu_0 \vec{j}$), where \vec{B} is the magnetic field vector, \vec{j} is the current density vector, and μ_0 is the magnetic permeability in the vacuum. Kivelson and Khurana (1995) include the axial magnetic field component (B_m). This model does not
135 consider the gradient of the magnetic field along the axis of the flux rope. The self-consistent solution of the flux rope model is



$$\begin{cases} B_{max} = \left(\frac{B_T}{\chi}\right) \sqrt{1 + \epsilon^2} \sinh\left(\frac{x_{min}}{T}\right) \\ B_{int} = \left(\frac{B_T}{\chi}\right) \sqrt{1 + \left(\frac{B_{int0}\chi}{B_T}\right)^2} \\ B_{min} = \left(\frac{B_T}{\chi}\right) \epsilon \sin\left(\frac{x_{max}}{T}\right) \end{cases} \quad (1)$$

140 In the equation, the parameter ϵ is associated with the shape of the flux rope. The x_{min} and x_{max} are the locations along with \vec{n}_{min} and \vec{n}_{max} . The T is the vertical scale of flux rope and the B_T is the magnetic field intensity near the boundary of the flux rope along with the \vec{n}_{min} . The B_{int0} is the B_{int} in the background. In this study, the \vec{n}_{min} , \vec{n}_{int} and \vec{n}_{max} refer to the local coordinate of each flux rope. The χ is

$$\chi = \epsilon \cos\left(\frac{x_{max}}{T}\right) + \sqrt{1 + \epsilon^2} \cosh\left(\frac{x_{min}}{T}\right) \quad (2)$$

The axial flux content (Φ_{axial}) is calculated by integrating the axial field (B_{int}) over the entire flux rope area,

$$\Phi_{axial} = \int B_{int} dS \quad (3)$$

During the fitting, we assume that the traveling speed of flux ropes was 100 km/s, which corresponds to the average Alfvén speed in the sub-solar magnetosheath. The least-squares of the minimization of the magnetic field differences (X^2) is employed to define the best fit, which is calculated from

$$X^2 = \frac{\sum_{i=1}^{N_{point}} \sum_j^{max,int,min} \left[\left(B_j(i) - B'_j(i) \right) / B_t(i) \right]^2}{N_{point}} \quad (4)$$

145 where B_{max} , B_{int} , B_{min} , and B_t are the components and magnitude of the measured magnetic fields and B'_{max} , B'_{int} , and B'_{min} are the components from the model. The N_{point} is the number of data points. We set up a threshold of $X^2 < 0.1$ to be the successful modeling.

Different from the circular profile of flux ropes resulted from the Lundquist force-free flux rope model (Lundquist, 1950), this force-free model gives a flattened profile of the flux rope. We use the semi-minor and semi-major to refer to the flatten features. This flux rope model is successfully applied for the flux ropes in the Earth's plasma sheet (Kivelson and Khurana, 1995), Earth's magnetopause (Zhang et al., 2008), and in Mercury's plasma sheet (Zhao et al., 2019).

155 Out of the 6 FTE-type flux ropes, 4 were successfully modeled. The modeling results were summarized in Table 1. In Figures 3a to 3d, the dashed lines overlapping with the solid measured magnetic fields represent the modeling curves from the flux rope model. The plasma density was $\sim 10 \text{ cm}^{-3}$ corresponding to an ion inertial length (d_i) of $\sim 70 \text{ km}$. The two FTE-type flux ropes centered at 00:26:06 UT and 00:26:26 UT were in the scales of several d_i . The magnetic flux content of these two flux ropes was small ($\sim 20 \text{ kWb}$). In addition, these two flux ropes corresponded to the largest and smallest core fields.

160 The other two FTE-type flux ropes centered at 00:28:13 UT and 00:30:26 UT were in the scales of more than $10 d_i$. These two flux ropes contained much higher magnetic flux ($\sim 300 \text{ kWb}$ and $\sim 188 \text{ kWb}$). The analysis of the flux rope centered at $\sim 00:28:13 \text{ UT}$ corresponding to the highest magnetic flux content is shown in the next.



3.4. Coalescence Event

Figure 3 shows that the magnetic field measurements of the FTE-type flux rope centered at $\sim 00:28:13$ UT in the LMN coordinate. Figure 3c showed the B_N included two successive bipolar signatures, which implied that two smaller scale flux ropes merging. Indeed, the hodogram in the B_{\max} - B_{int} plane in Figure 3f confirmed the field rotations of two flux ropes, named “FR#A” and “FR#B”. Figure 3e further illustrated the merging of FR#A and FR#B, and the trajectory of BepiColombo. The magenta arrows and shaded region in Figure 3e indicated the secondary reconnection between FR#A and FR#B. This FTE-type flux rope with the highest flux content was cleared resulted from the coalescence of two smaller-scale flux ropes.

It needs to note that the coalescence signature is only observed in this FTE-type flux rope. We did not see similar successive bipolar signatures of the B_N in other 5 FTE-type flux ropes.

3.5. Magnetopause Reconnection and Secondary Magnetic Reconnection

In Figure 4, the reconnection properties of the secondary reconnecting current sheet in the coalescence event (Figure 3) and the magnetopause current sheet are studied. For the secondary reconnecting current sheet, the ratios of $\lambda_{\max}/\lambda_{\text{int}} \sim 6.4$, $\lambda_{\text{int}}/\lambda_{\text{min}} \sim 11.0$ resulted from MVA were both larger than 3 indicating the local coordinate of the secondary reconnecting current was well built. The magnetic field measurements of the magnetopause current sheet were shown in the LMN coordinate.

In the reconnecting current sheet, the dimensionless reconnection rate can be determined from the ratio of normal magnetic field component (B_{normal}) to the reconnecting magnetic field (B_{inflow}) in the inflow region (Sonnerup, 1974; Sonnerup et al., 1981; Fuselier and Lewis, 2011; Phan et al., 2001). In the secondary reconnecting current sheet (Figures 4a to 4d), the B_{normal} was ~ 5 nT (the B_{min} averaged from 00:28:08.8 to 00:28:09.6 UT). Here the average B_t from 00:28:09.8 to 00:28:10.4 UT was taken as the B_{inflow} (~ 36 nT). The dimensionless reconnection rate was ~ 0.14 . Meanwhile, the intensity of the guide field (B_{int} , Figure 4b) was ~ 32 nT across the current sheet, which was ~ 0.89 when normalized to the B_{inflow} . However, it needs to point out that the estimation of reconnection rate based on B_N/B_{inflow} could be imprecise. For example, the uncertainties of the normal direction and the fluctuations in the field strength could influence the accuracy of the reconnection rates.

In the magnetopause current sheet, the B_{normal} was 8.3 nT (averaged B_N from 00:32:56 to 00:33:05 UT, Figure 4g). The B_{inflow} in the magnetosphere side adjacent to the magnetopause was ~ 46.1 nT (average B_t from 00:33:06 to 00:33:15 UT, Figure 4h). Thus, the dimensionless reconnection rate was calculated to be ~ 0.18 . The guide field across the magnetopause was ~ 13 nT, which was 0.28 normalized to the B_{inflow} .

4. Conclusions and Discussions

Our analysis of the subsolar magnetopause observations during BepiColombo’s Earth flyby was produced several conclusions.

First, the BepiColombo’s dayside magnetopause crossing corresponds to the magnetosheath with high plasma β (~ 8) and a significant radial component of the IMF ($B_x/B_{\text{tot}} > 0.75$). The traveling of the FTE-type flux rope suggests that the X-line crosses the location of BepiColombo, which is verified by the motion of the X-lines obtained from



the maximum magnetic shear model. The motion of the X-line is associated with the rotation and the increase in the B_x of the IMF. BepiColombo crosses the magnetopause near the magnetic equator, and 10 April 2020 is close to the spring equinox, which indicates a small dipole tilt influence. These observations of the crossing of the X-line provide clear evidence of magnetic reconnection near the magnetic equator under a strong radial IMF.

Second, the properties of the FTE-type flux ropes are determined by employing a flux rope model. The FTE-type flux ropes have scales ranging from several d_i to around $20 d_i$, and the FTE-type flux rope with a large scale and the highest magnetic flux content corresponds to a clear coalescence signature. This observation strongly supports a key feature that the FTE-type flux rope can grow in scale and magnetic flux content through coalescence.

Third, the features of magnetic reconnection associated with the secondary reconnection in the coalescence event and the magnetopause current sheet are investigated. The reconnection rate of the secondary reconnection (0.14) is comparable with the reconnection rate on the dayside magnetopause (0.18). However, the secondary reconnection corresponds to a larger normalized guide field (0.89) than the magnetopause reconnection (0.28). The large guide field is likely a common feature for the secondary magnetic reconnection during the coalescence.

Using the MMS measurements, Zhou et al. (2017) reported a coalescence event with a strong guide field. We suggest that the large guide field shall be considered in the simulations, which investigate the particle energizations due to the coalescence. For example, the large guide field may influence the reconnection rate as suggested by Pritchett and Coroniti (2004) and Ricci et al. (2004), and therefore influences the energization of particles during the coalescence. Furthermore, a recent investigation also suggests that a large guide field might limit the ability of Fermi acceleration during the coalescence (Montag et al., 2017).

The FTE-type flux rope containing coalescence signature has a scale of $\sim 20 d_i$. Therefore, the secondary reconnecting current sheet embedded within the FTE-type flux rope is likely with scale much smaller than $20 d_i$. We want to note that the secondary reconnection during the coalescence of flux ropes share some similarities with the electron-only reconnection the magnetosheath turbulence, whose reconnecting current sheet has scales ($< 10 d_i$) and a large guide field as revealed by MMS measurements (Phan et al., 2018; Stawarz et al., 2019) and simulations (Califano et al., 2020). Therefore, it is likely that the secondary reconnection associated with coalescence is also electron-only magnetic reconnection, which certainly deserves a detail study.

Data availability

The measurements from Mio/MEA and MPO/MAG analyzed in this study are available in the supporting information. The data archiving is underway. Mio/MEA data will be able to be accessed from the AMDA science analysis system (<http://amda.cdpp.eu>) provided by the Centre de Données de la Physique des Plasmas (CDPP) supported by CNRS, CNES, Observatoire de Paris, and Université Paul Sabatier Toulouse. MPO/MAG data will be available from <https://archives.esac.esa.int/psa/#!/Home%20View>. OMNI dataset is available at <https://omniweb.gsfc.nasa.gov/>.



Author contributions

235 W. J. S. led the work, identified the events, conducted the data analysis of the dataset, and wrote the manuscript. W. J. S., J. A. S. and R. N. jointly designed the work. D. H. and J. Z. D. M. provided knowledge of the MPO-MAG instrument and the MPO-MAG data. S. A. and N. A. provided knowledge of the Mio-MEA instrument and the Mio-MEA data. K. J. T. provided Figure 3 and the relevant descriptions. J. T. Z. performed force-free fittings of the flux ropes. All authors discussed and contributed to the manuscript.

240

Competing interests

The authors declare no competing interests.

Acknowledgment

245 The BepiColombo project is supported by ESA and JAXA. W. J. S. and J. A. S. were supported by NASA Grants NNX16AJ67G and 80NSSC18K1137. N.A. and S.A. acknowledge the support of CNES for the BepiColombo mission. The research at LASP (K. J. T.) is supported by NASA grant NNG04EB99C and 80NSSC20K0688. W. J. S. thanks Dr. Gangkai Poh for helpful discussions.

References.

- 250 Akhavan-Tafti, M., Slavin, J. A., Le, G., Eastwood, J. P., Strangeway, R. J., Russell, C. T., Nakamura, R., Baumjohann, W., Torbert, R. B., Giles, B. L., Gershman, D. J., and Burch, J. L.: MMS Examination of FTEs at the Earth's Subsolar Magnetopause, *J Geophys Res Space Phys*, 123, 1224-1241, 10.1002/2017JA024681, 2018.
- Belenkaya, E. S.: Reconnection modes for near-radial interplanetary magnetic field, *J Geophys Res Space Phys*, 103, 26487-26494, <https://doi.org/10.1029/98JA02270>, 1998.
- 255 Benkhoff, J., van Casteren, J., Hayakawa, H., Fujimoto, M., Laakso, H., Novara, M., Ferri, P., Middleton, H. R., and Ziethe, R.: BepiColombo—Comprehensive exploration of Mercury: Mission overview and science goals, *Planet Space Sci*, 58, 2-20, <https://doi.org/10.1016/j.pss.2009.09.020>, 2010.
- Biskamp, D. and Welter, H.: Coalescence of Magnetic Islands, *Phys Rev Lett*, 44, 1069-1072, 10.1103/PhysRevLett.44.1069, 1980.
- 260 Burch, J. L., Moore, T. E., Torbert, R. B., and Giles, B. L.: Magnetospheric Multiscale Overview and Science Objectives, *Space Sci Rev*, 199, 5-21, 10.1007/s11214-015-0164-9, 2016.
- Califano, F., Cerri, S. S., Faganello, M., Laveder, D., Sisti, M., and Kunz, M. W.: Electron-Only Reconnection in Plasma Turbulence, *Front Phys*, 8, 10.3389/fphy.2020.00317, 2020.
- 265 Dorelli, J. C. and Bhattacharjee, A.: On the generation and topology of flux transfer events, *J Geophys Res Space Phys*, 114, <https://doi.org/10.1029/2008JA013410>, 2009.
- Drake, J. F., Swisdak, M., Che, H., and Shay, M. A.: Electron acceleration from contracting magnetic islands during reconnection, *Nature*, 443, 553, 10.1038/nature05116, 2006.



- Dungey, J. W.: Interplanetary Magnetic Field and the Auroral Zones, *Phys Rev Lett*, 6, 47-48,
270 10.1103/PhysRevLett.6.47, 1961.
- Fear, R. C., Trenchi, L., Coxon, J. C., and Milan, S. E.: How Much Flux Does a Flux Transfer Event Transfer?, *J Geophys Res Space Phys*, 122, 12,310-312,327, doi:10.1002/2017JA024730, 2017.
- Fermo, R. L., Drake, J. F., Swisdak, M., and Hwang, K. J.: Comparison of a statistical model for magnetic islands in large current layers with Hall MHD simulations and Cluster FTE observations, *J Geophys Res Space Phys*, 116,
275 10.1029/2010JA016271, 2011.
- Fuselier, S. A. and Lewis, W. S.: Properties of Near-Earth Magnetic Reconnection from In-Situ Observations, *Space Sci Rev*, 160, 95, 10.1007/s11214-011-9820-x, 2011.
- Heyner, D., Auster, H. U., Fornaçon, K. H., Carr, C., Richter, I., Mieth, J. Z. D., Kolhey, P., Exner, W., Motschmann, U., Baumjohann, W., Matsuoka, A., Magnes, W., Berghofer, G., Fischer, D., Plaschke, F., Nakamura,
280 R., Narita, Y., Delva, M., Volwerk, M., Balogh, A., Dougherty, M., Horbury, T., Langlais, B., Manda, M., Masters, A., Oliveira, J. S., Sánchez-Cano, B., Slavin, J. A., Vennerstrøm, S., Vogt, J., Wicht, J., and Glassmeier, K. H.: The BepiColombo Planetary Magnetometer MPO-MAG: What Can We Learn from the Hermean Magnetic Field?, *Space Sci Rev*, 217, 52, 10.1007/s11214-021-00822-x, 2021.
- Hoilijoki, S., Ganse, U., Pfau-Kempf, Y., Cassak, P. A., Walsh, B. M., Hietala, H., von Althaus, S., and Palmroth,
285 M.: Reconnection rates and X line motion at the magnetopause: Global 2D-3V hybrid-Vlasov simulation results, *J Geophys Res Space Phys*, 122, 2877-2888, <https://doi.org/10.1002/2016JA023709>, 2017.
- Imber, S. M., Slavin, J. A., Boardsen, S. A., Anderson, B. J., Korth, H., McNutt Jr., R. L., and Solomon, S. C.: MESSENGER observations of large dayside flux transfer events: Do they drive Mercury's substorm cycle?, *J Geophys Res Space Phys*, 119, 5613-5623, 10.1002/2014ja019884, 2014.
- 290 Jasinski, J. M., Akhavan-Tafti, M., Sun, W., Slavin, J. A., Coates, A. J., Fuselier, S. A., Sergis, N., and Murphy, N.: Flux Transfer Events at a Reconnection-Suppressed Magnetopause: Cassini Observations at Saturn, *J Geophys Res Space Phys*, 126, e2020JA028786, <https://doi.org/10.1029/2020JA028786>, 2021.
- Jasinski, J. M., Slavin, J. A., Arridge, C. S., Poh, G., Jia, X., Sergis, N., Coates, A. J., Jones, G. H., and Waite Jr., J. H.: Flux transfer event observation at Saturn's dayside magnetopause by the Cassini spacecraft, *Geophys Res Lett*,
295 43, 6713-6723, doi:10.1002/2016GL069260, 2016.
- Kacem, I., Jacquy, C., Génot, V., Lavraud, B., Vernisse, Y., Marchaudon, A., Le Contel, O., Breuillard, H., Phan, T. D., Hasegawa, H., Oka, M., Trattner, K. J., Farrugia, C. J., Paulson, K., Eastwood, J. P., Fuselier, S. A., Turner, D., Eriksson, S., Wilder, F., Russell, C. T., Øieroset, M., Burch, J., Graham, D. B., Sauvaud, J. A., Avannov, L., Chandler, M., Coffey, V., Dorelli, J., Gershman, D. J., Giles, B. L., Moore, T. E., Saito, Y., Chen, L. J., and Penou,
300 E.: Magnetic Reconnection at a Thin Current Sheet Separating Two Interlaced Flux Tubes at the Earth's Magnetopause, *J Geophys Res Space Phys*, 123, 1779-1793, 10.1002/2017JA024537, 2018.
- King, J. H. and Papitashvili, N. E.: Solar wind spatial scales in and comparisons of hourly Wind and ACE plasma and magnetic field data, *J Geophys Res Space Phys*, 110, 10.1029/2004ja010649, 2005.



- 305 Kivelson, M. G. and Khurana, K. K.: Models of flux ropes embedded in a harris neutral sheet: Force-free solutions in low and high beta plasmas, *J Geophys Res Space Phys*, 100, 23637-23645, <https://doi.org/10.1029/95JA01548>, 1995.
- Kuo, H., Russell, C. T., and Le, G.: Statistical studies of flux transfer events, *J Geophys Res Space Phys*, 100, 3513-3519, <https://doi.org/10.1029/94JA02498>, 1995.
- 310 Lai, H. R., Wei, H. Y., Russell, C. T., Arridge, C. S., and Dougherty, M. K.: Reconnection at the magnetopause of Saturn: Perspective from FTE occurrence and magnetosphere size, *J Geophys Res Space Phys*, 117, 10.1029/2011ja017263, 2012.
- Lee, L. C. and Fu, Z. F.: A theory of magnetic flux transfer at the Earth's magnetopause, *Geophys Res Lett*, 12, 105-108, 10.1029/GL012i002p00105, 1985.
- 315 Lee, L. C., Ma, Z. W., Fu, Z. F., and Otto, A.: Topology of magnetic flux ropes and formation of fossil flux transfer events and boundary layer plasmas, *J Geophys Res Space Phys*, 98, 3943-3951, <https://doi.org/10.1029/92JA02203>, 1993.
- Lockwood, M., Cowley, S. W. H., Smith, M. F., Rijnbeek, R. P., and Elphic, R. C.: The contribution of flux transfer events to convection, *Geophys Res Lett*, 22, 1185-1188, 10.1029/95gl01008, 1995.
- 320 Luhmann, J. G., Walker, R. J., Russell, C. T., Crooker, N. U., Spreiter, J. R., and Stahara, S. S.: Patterns of potential magnetic field merging sites on the dayside magnetopause, *J Geophys Res Space Phys*, 89, 1739-1742, <https://doi.org/10.1029/JA089iA03p01739>, 1984.
- Lundquist, S.: Magnetohydrostatic fields, *Ark. Fys.*, 2, 361-365, 1950.
- Mangano, V., Dósa, M., Fränz, M., Milillo, A., Oliveira, J. S., Lee, Y. J., McKenna-Lawlor, S., Grassi, D., Heyner, D., Kozyrev, A. S., Peron, R., Helbert, J., Besse, S., de la Fuente, S., Montagnon, E., Zender, J., Volwerk, M.,
- 325 Chaufray, J.-Y., Slavin, J. A., Krüger, H., Maturilli, A., Cornet, T., Iwai, K., Miyoshi, Y., Lucente, M., Massetti, S., Schmidt, C. A., Dong, C., Quarati, F., Hirai, T., Varsani, A., Belyaev, D., Zhong, J., Kilpua, E. K. J., Jackson, B. V., Odstrcil, D., Plaschke, F., Vainio, R., Jarvinen, R., Ivanovski, S. L., Madár, Á., Erdős, G., Plainaki, C., Alberti, T., Aizawa, S., Benkhoff, J., Murakami, G., Quémérais, E., Hiesinger, H., Mitrofanov, I. G., Iess, L., Santoli, F., Orsini, S., Lichtenegger, H., Laky, G., Barabash, S., Moissl, R., Huovelin, J., Kasaba, Y., Saito, Y., Kobayashi, M., and
- 330 Baumjohann, W.: BepiColombo Science Investigations During Cruise and Flybys at the Earth, Venus and Mercury, *Space Sci Rev*, 217, 23, 10.1007/s11214-021-00797-9, 2021.
- Milillo, A., Fujimoto, M., Murakami, G., Benkhoff, J., Zender, J., Aizawa, S., Dósa, M., Griton, L., Heyner, D., Ho, G., Imber, S. M., Jia, X., Karlsson, T., Killen, R. M., Laurenza, M., Lindsay, S. T., McKenna-Lawlor, S., Mura, A., Raines, J. M., Rothery, D. A., André, N., Baumjohann, W., Berezhnoy, A., Bourdin, P. A., Bunce, E. J., Califano, F., Deca, J., de la Fuente, S., Dong, C., Grava, C., Fatemi, S., Henri, P., Ivanovski, S. L., Jackson, B. V., James, M.,
- 335 Kallio, E., Kasaba, Y., Kilpua, E., Kobayashi, M., Langlais, B., Leblanc, F., Lhotka, C., Mangano, V., Martindale, A., Massetti, S., Masters, A., Morooka, M., Narita, Y., Oliveira, J. S., Odstrcil, D., Orsini, S., Pelizzo, M. G., Plainaki, C., Plaschke, F., Sahraoui, F., Seki, K., Slavin, J. A., Vainio, R., Wurz, P., Barabash, S., Carr, C. M., Delcourt, D., Glassmeier, K. H., Grande, M., Hirahara, M., Huovelin, J., Korabely, O., Kojima, H., Lichtenegger, H., Livi, S., Matsuoka, A., Moissl, R., Moncuquet, M., Muinonen, K., Quémérais, E., Saito, Y., Yagitani, S.,



- Yoshikawa, I., and Wahlund, J. E.: Investigating Mercury's Environment with the Two-Spacecraft BepiColombo Mission, *Space Sci Rev*, 216, 93, 10.1007/s11214-020-00712-8, 2020.
- Montag, P., Egedal, J., Lichko, E., and Wetherton, B.: Impact of compressibility and a guide field on Fermi acceleration during magnetic island coalescence, *Phys Plasmas*, 24, 062906, 10.1063/1.4985302, 2017.
- 345 Murakami, G., Hayakawa, H., Ogawa, H., Matsuda, S., Seki, T., Kasaba, Y., Saito, Y., Yoshikawa, I., Kobayashi, M., Baumjohann, W., Matsuoka, A., Kojima, H., Yagitani, S., Moncuquet, M., Wahlund, J.-E., Delcourt, D., Hirahara, M., Barabash, S., Korablev, O., and Fujimoto, M.: Mio—First Comprehensive Exploration of Mercury's Space Environment: Mission Overview, *Space Sci Rev*, 216, 113, 10.1007/s11214-020-00733-3, 2020.
- 350 Øieroset, M., Phan, T. D., Haggerty, C., Shay, M. A., Eastwood, J. P., Gershman, D. J., Drake, J. F., Fujimoto, M., Ergun, R. E., Mozer, F. S., Oka, M., Torbert, R. B., Burch, J. L., Wang, S., Chen, L. J., Swisdak, M., Pollock, C., Dorelli, J. C., Fuselier, S. A., Lavraud, B., Giles, B. L., Moore, T. E., Saito, Y., Avanov, L. A., Paterson, W., Strangeway, R. J., Russell, C. T., Khotyaintsev, Y., Lindqvist, P. A., and Malakit, K.: MMS observations of large guide field symmetric reconnection between colliding reconnection jets at the center of a magnetic flux rope at the magnetopause, *Geophys Res Lett*, 43, 5536-5544, <https://doi.org/10.1002/2016GL069166>, 2016.
- 355 Paschmann, G., Haerendel, G., Papamastorakis, I., Scokpe, N., Bame, S. J., Gosling, J. T., and Russell, C. T.: Plasma and magnetic field characteristics of magnetic flux transfer events, *J Geophys Res Space Phys*, 87, 2159-2168, <https://doi.org/10.1029/JA087iA04p02159>, 1982.
- Phan, T. D., Sonnerup, B. U. Ö., and Lin, R. P.: Fluid and kinetics signatures of reconnection at the dawn tail magnetopause: Wind observations, *J Geophys Res Space Phys*, 106, 25489-25501, <https://doi.org/10.1029/2001JA900054>, 2001.
- 360 Phan, T. D., Eastwood, J. P., Shay, M. A., Drake, J. F., Sonnerup, B. U. Ö., Fujimoto, M., Cassak, P. A., Øieroset, M., Burch, J. L., Torbert, R. B., Rager, A. C., Dorelli, J. C., Gershman, D. J., Pollock, C., Pyakurel, P. S., Haggerty, C. C., Khotyaintsev, Y., Lavraud, B., Saito, Y., Oka, M., Ergun, R. E., Retino, A., Le Contel, O., Argall, M. R., Giles, B. L., Moore, T. E., Wilder, F. D., Strangeway, R. J., Russell, C. T., Lindqvist, P. A., and Magnes, W.:
- 365 Electron magnetic reconnection without ion coupling in Earth's turbulent magnetosheath, *Nature*, 557, 202-206, 10.1038/s41586-018-0091-5, 2018.
- Pi, G., Shue, J.-H., Grygorov, K., Li, H.-M., Němeček, Z., Šafránková, J., Yang, Y.-H., and Wang, K.: Evolution of the magnetic field structure outside the magnetopause under radial IMF conditions, *J Geophys Res Space Phys*, 122, 4051-4063, <https://doi.org/10.1002/2015JA021809>, 2017.
- 370 Pritchett, P. L. and Coroniti, F. V.: Three-dimensional collisionless magnetic reconnection in the presence of a guide field, *J Geophys Res Space Phys*, 109, 10.1029/2003ja009999, 2004.
- Raeder, J.: Flux Transfer Events: 1. generation mechanism for strong southward IMF, *Ann. Geophys.*, 24, 381-392, 10.5194/angeo-24-381-2006, 2006.
- 375 Ricci, P., Brackbill, J. U., Daughton, W., and Lapenta, G.: Collisionless magnetic reconnection in the presence of a guide field, *Phys Plasmas*, 11, 4102-4114, 10.1063/1.1768552, 2004.



- Rijnbeek, R. P., Cowley, S. W. H., Southwood, D. J., and Russell, C. T.: A survey of dayside flux transfer events observed by ISEE 1 and 2 magnetometers, *J Geophys Res Space Phys*, 89, 786-800, 10.1029/JA089iA02p00786, 1984.
- Russell, C. T. and Elphic, R. C.: Initial ISEE magnetometer results: magnetopause observations, *Space Sci Rev*, 22, 681-715, 10.1007/BF00212619, 1978.
- 380 Russell, C. T. and Walker, R. J.: Flux transfer events at Mercury, *J Geophys Res Space Phys*, 90, 11067-11074, 10.1029/JA090iA11p11067, 1985.
- Saito, Y., Delcourt, D., Hirahara, M., Barabash, S., André, N., Takashima, T., Asamura, K., Yokota, S., Wieser, M., Nishino, M. N., Oka, M., Futaana, Y., Harada, Y., Sauvaud, J.-A., Louarn, P., Lavraud, B., Génot, V., Mazelle, C., Dandouras, I., Jacquy, C., Aoustin, C., Barthe, A., Cadu, A., Fedorov, A., Frezoul, A.-M., Garat, C., Le Comte, E., Lee, Q.-M., Médale, J.-L., Moirin, D., Penou, E., Petiot, M., Peyre, G., Rouzaud, J., Séran, H.-C., Němeček, Z., Šafránková, J., Marcucci, M. F., Bruno, R., Consolini, G., Miyake, W., Shinohara, I., Hasegawa, H., Seki, K., Coates, A. J., Leblanc, F., Verdeil, C., Katra, B., Fontaine, D., Illiano, J.-M., Berthelier, J.-J., Techer, J.-D., Fraenz, M., Fischer, H., Krupp, N., Woch, J., Bührke, U., Fiethe, B., Michalik, H., Matsumoto, H., Yanagimachi, T., Miyoshi, Y., Mitani, T., Shimoyama, M., Zong, Q., Wurz, P., Andersson, H., Karlsson, S., Holmström, M., Kazama, Y., Ip, W.-H., Hoshino, M., Fujimoto, M., Terada, N., Keika, K., and BepiColombo Mio, M. T.: Pre-flight Calibration and Near-Earth Commissioning Results of the Mercury Plasma Particle Experiment (MPPE) Onboard MMO (Mio), *Space Sci Rev*, 217, 70, 10.1007/s11214-021-00839-2, 2021.
- Saunders, M. A., Russell, C. T., and Sckopke, N.: Flux transfer events: Scale size and interior structure, *Geophys Res Lett*, 11, 131-134, 10.1029/GL011i002p00131, 1984.
- 395 Sauvaud, J. A., Fedorov, A., Aoustin, C., Seran, H. C., Le Comte, E., Petiot, M., Rouzaud, J., Saito, Y., Dandouras, J., Jacquy, C., Louarn, P., Mazelle, C., and Médale, J. L.: The Mercury Electron Analyzers for the Bepi Colombo mission, *Adv Space Res*, 46, 1139-1148, <https://doi.org/10.1016/j.asr.2010.05.022>, 2010.
- Schindler, K., Pfirsich, D., and Wobig, H.: Stability of two-dimensional collision-free plasmas, *Plasma Phys*, 15, 1165-1184, 10.1088/0032-1028/15/12/001, 1973.
- 400 Shi, Q. Q., Zong, Q. G., Zhang, H., Pu, Z. Y., Fu, S. Y., Xie, L., Wang, Y. F., Chen, Y., Li, L., Xia, L. D., Liu, Z. X., Fazakerley, A. N., Reme, H., and Lucek, E.: Cluster observations of the entry layer equatorward of the cusp under northward interplanetary magnetic field, *J Geophys Res Space Phys*, 114, 10.1029/2009JA014475, 2009.
- Shi, Q. Q., Zong, Q. G., Fu, S. Y., Dunlop, M. W., Pu, Z. Y., Parks, G. K., Wei, Y., Li, W. H., Zhang, H., Nowada, M., Wang, Y. B., Sun, W. J., Xiao, T., Reme, H., Carr, C., Fazakerley, A. N., and Lucek, E.: Solar wind entry into the high-latitude terrestrial magnetosphere during geomagnetically quiet times, *Nat Commun*, 4, 1466, 10.1038/ncomms2476, 2013.
- Slavin, J. A., Imber, S. M., Boardsen, S. A., DiBraccio, G. A., Sundberg, T., Sarantos, M., Nieves-Chinchilla, T., Szabo, A., Anderson, B. J., Korth, H., Zurbuchen, T. H., Raines, J. M., Johnson, C. L., Winslow, R. M., Killen, R. M., McNutt Jr., R. L., and Solomon, S. C.: MESSENGER observations of a flux-transfer-event shower at Mercury, *J Geophys Res Space Phys*, 117, 10.1029/2012ja017926, 2012.
- 410



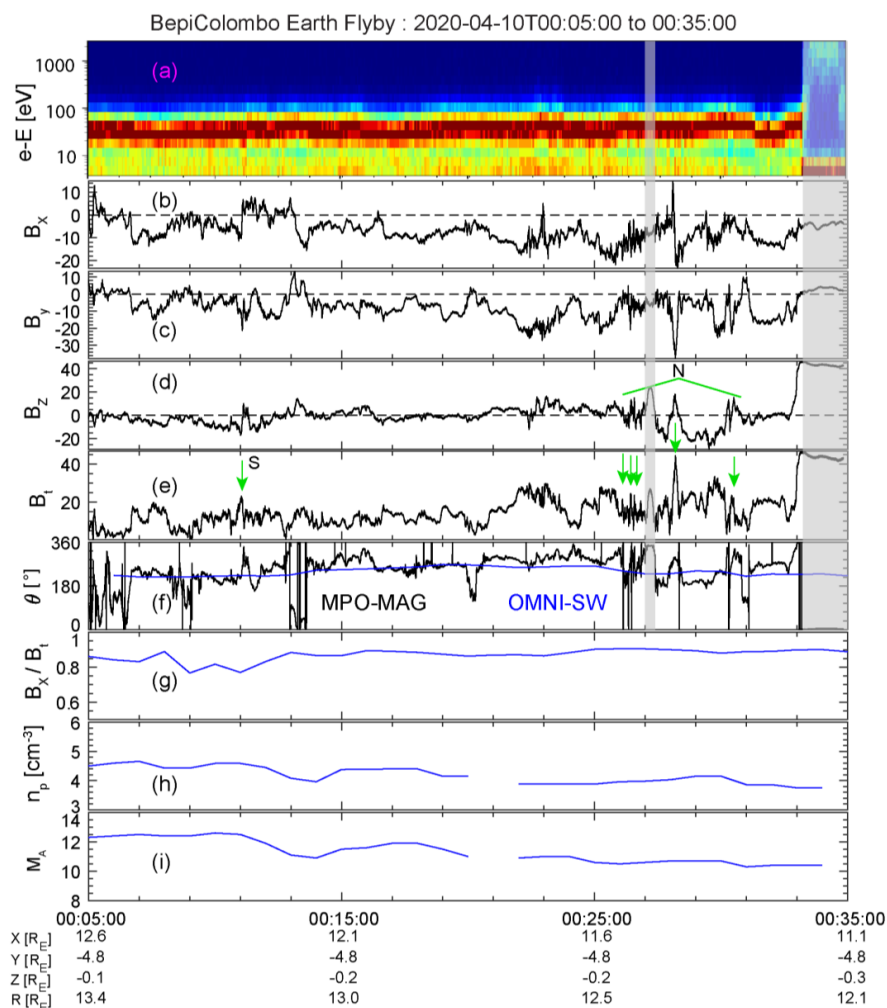
- Slavin, J. A., Lepping, R. P., Wu, C.-C., Anderson, B. J., Baker, D. N., Benna, M., Boardsen, S. A., Killen, R. M., Korth, H., Krimigis, S. M., McClintock, W. E., McNutt Jr., R. L., Sarantos, M., Schriver, D., Solomon, S. C., Trávníček, P., and Zurbuchen, T. H.: MESSENGER observations of large flux transfer events at Mercury, *Geophys Res Lett*, 37, 10.1029/2009gl041485, 2010.
- 415 Slavin, J. A., Acuña, M. H., Anderson, B. J., Baker, D. N., Benna, M., Boardsen, S. A., Gloeckler, G., Gold, R. E., Ho, G. C., Korth, H., Krimigis, S. M., McNutt, R. L., Raines, J. M., Sarantos, M., Schriver, D., Solomon, S. C., Trávníček, P., and Zurbuchen, T. H.: MESSENGER Observations of Magnetic Reconnection in Mercury's Magnetosphere, *Science*, 324, 606, 10.1126/science.1172011, 2009.
- 420 Song, P. and Russell, C. T.: Model of the formation of the low-latitude boundary layer for strongly northward interplanetary magnetic field, *J Geophys Res Space Phys*, 97, 1411-1420, <https://doi.org/10.1029/91JA02377>, 1992.
- Sonnerup, B. U. Ö.: Magnetopause reconnection rate, *J Geophys Res*, 79, 1546-1549, 10.1029/JA079i010p01546, 1974.
- Sonnerup, B. U. Ö. and Cahill Jr., L. J.: Magnetopause structure and attitude from Explorer 12 observations, *J Geophys Res*, 72, 171-183, 10.1029/JZ072i001p00171, 1967.
- 425 Sonnerup, B. U. Ö. and Scheible, M.: Minimum and maximum variance analysis, in: Analysis methods for multi-spacecraft data, edited by: Paschmann, G., and Daly, P. W., ESA Publication, Noordwijk, Netherlands., 185-220, 1998.
- Sonnerup, B. U. Ö., Paschmann, G., Papamastorakis, I., Sckopke, N., Haerendel, G., Bame, S. J., Asbridge, J. R., Gosling, J. T., and Russell, C. T.: Evidence for magnetic field reconnection at the Earth's magnetopause, *J Geophys Res Space Phys*, 86, 10049-10067, 10.1029/JA086iA12p10049, 1981.
- 430 Stawarz, J. E., Eastwood, J. P., Phan, T. D., Gingell, I. L., Shay, M. A., Burch, J. L., Ergun, R. E., Giles, B. L., Gershman, D. J., Contel, O. L., Lindqvist, P. A., Russell, C. T., Strangeway, R. J., Torbert, R. B., Argall, M. R., Fischer, D., Magnes, W., and Franci, L.: Properties of the Turbulence Associated with Electron-only Magnetic Reconnection in Earth's Magnetosheath, *Astrophys J*, 877, L37, 10.3847/2041-8213/ab21c8, 2019.
- 435 Sun, W. J., Slavin, J. A., Smith, A. W., Dewey, R. M., Poh, G. K., Jia, X., Raines, J. M., Livi, S., Saito, Y., Gershman, D. J., DiBraccio, G. A., Imber, S. M., Guo, J. P., Fu, S. Y., Zong, Q. G., and Zhao, J. T.: Flux Transfer Event Showers at Mercury: Dependence on Plasma β and Magnetic Shear and Their Contribution to the Dungey Cycle, *Geophys Res Lett*, 47, e2020GL089784, <https://doi.org/10.1029/2020GL089784>, 2020.
- 440 Tang, B. B., Wang, C., and Li, W. Y.: The magnetosphere under the radial interplanetary magnetic field: A numerical study, *J Geophys Res Space Phys*, 118, 7674-7682, <https://doi.org/10.1002/2013JA019155>, 2013.
- Trattner, K. J., Mulcock, J. S., Petrinec, S. M., and Fuselier, S. A.: Probing the boundary between antiparallel and component reconnection during southward interplanetary magnetic field conditions, *J Geophys Res Space Phys*, 112, <https://doi.org/10.1029/2007JA012270>, 2007.
- 445 Trattner, K. J., Petrinec, S. M., Fuselier, S. A., and Phan, T. D.: The location of reconnection at the magnetopause: Testing the maximum magnetic shear model with THEMIS observations, *J Geophys Res Space Phys*, 117, <https://doi.org/10.1029/2011JA016959>, 2012.



- Trattner, K. J., Fuselier, S. A., Petrinec, S. M., Burch, J. L., Ergun, R., and Grimes, E. W.: Long and Active Magnetopause Reconnection X-Lines During Changing IMF Conditions, *J Geophys Res Space Phys*, 126, e2020JA028926, <https://doi.org/10.1029/2020JA028926>, 2021.
- 450
- Trattner, K. J., Burch, J. L., Ergun, R., Eriksson, S., Fuselier, S. A., Giles, B. L., Gomez, R. G., Grimes, E. W., Lewis, W. S., Mauk, B., Petrinec, S. M., Russell, C. T., Strangeway, R. J., Trenchi, L., and Wilder, F. D.: The MMS Dayside Magnetic Reconnection Locations During Phase 1 and Their Relation to the Predictions of the Maximum Magnetic Shear Model, *J Geophys Res Space Phys*, 122, 11,991-912,005, <https://doi.org/10.1002/2017JA024488>,
- 455
- 2017.
- Walker, R. J. and Russell, C. T.: Flux transfer events at the Jovian magnetopause, *J Geophys Res Space Phys*, 90, 7397-7404, 10.1029/JA090iA08p07397, 1985.
- Wang, Y. L., Elphic, R. C., Lavraud, B., Taylor, M. G. G. T., Birn, J., Russell, C. T., Raeder, J., Kawano, H., and Zhang, X. X.: Dependence of flux transfer events on solar wind conditions from 3 years of Cluster observations, *J Geophys Res Space Phys*, 111, doi:10.1029/2005JA011342, 2006.
- 460
- Wang, Y. L., Elphic, R. C., Lavraud, B., Taylor, M. G. G. T., Birn, J., Raeder, J., Russell, C. T., Kawano, H., Zong, Q.-G., Zhang, H., Zhang, X. X., and Friedel, R. H.: Initial results of high-latitude magnetopause and low-latitude flank flux transfer events from 3 years of Cluster observations, *J Geophys Res Space Phys*, 110, doi:10.1029/2005JA011150, 2005.
- 465
- Zhang, H., Khurana, K. K., Kivelson, M. G., Angelopoulos, V., Pu, Z. Y., Zong, Q.-G., Liu, J., and Zhou, X.-Z.: Modeling a force-free flux transfer event probed by multiple Time History of Events and Macroscale Interactions during Substorms (THEMIS) spacecraft, *J Geophys Res Space Phys*, 113, 10.1029/2008ja013451, 2008.
- Zhao, J. T., Sun, W.-J., Zong, Q. G., Slavin, J. A., Zhou, X. Z., Dewey, R. M., Poh, G. K., and Raines, J. M.: A Statistical Study of the Force Balance and Structure in the Flux Ropes in Mercury's Magnetotail, *J Geophys Res Space Phys*, 124, 5143-5157, 10.1029/2018ja026329, 2019.
- 470
- Zhou, M., Berchem, J., Walker, R. J., El-Alaoui, M., Deng, X., Cazzola, E., Lapenta, G., Goldstein, M. L., Paterson, W. R., Pang, Y., Ergun, R. E., Lavraud, B., Liang, H., Russell, C. T., Strangeway, R. J., Zhao, C., Giles, B. L., Pollock, C. J., Lindqvist, P. A., Marklund, G., Wilder, F. D., Khotyaintsev, Y. V., Torbert, R. B., and Burch, J. L.: Coalescence of Macroscopic Flux Ropes at the Subsolar Magnetopause: Magnetospheric Multiscale Observations,
- 475
- Phys Rev Lett*, 119, 055101, 10.1103/PhysRevLett.119.055101, 2017.



Figures and Tables



480 **Figure 1. The electrons and magnetic field measurements of the dayside magnetopause.** (a) the time-energy
 spectrogram of normalized electron counts from Mio/MEA, (b) B_x , (c) B_y , (d) B_z , (e) the magnetic field intensity, B_t ,
 (f) the clock angle (θ), solar wind ratio of B_x/B_t (g), number density (n_p) (h), Alfvénic Mach number (M_A) (i). The
 485 black lines are from MPO/MAG, and the blue lines are from the OMNI. All quantities are in the Geocentric Solar
 Magnetospheric (GSM) coordinate. The θ in (f) is defined as $\arctan(B_y/B_z)$, ranging from 0° to 360° . The green
 arrows in (e) indicate the six FTE-type flux ropes. “S” indicates southward traveling and “N” northward traveling.



Table 1. List and properties of FTE-type flux ropes observed during BepiColombo's dayside magnetopause crossing

#	Time	Duration (s)	Travelling Direction	Core Field Intensity (nT)	Scale (km) ^b	Flux Content (kwb)	χ^2
1	00:11:03	~ 12	Southward	— ^a	—	—	—
2	00:26:06	~ 7	Northward	~23.9	~462, 388	~13.7	~0.04
3	00:26:26	~ 6	Northward	~60.8	~565, 524	~22.5	~0.04
4	00:26:35	~ 4	Northward	—	—	—	—
5	00:28:13	~ 20	Northward	~41	~1745, 1281	~300	~0.08
6	00:30:26	~ 15	Northward	~45.2	~1853,1745	~188	~0.08

490 ^a “—” indicate that the values are not determined by the flux rope model. See the text for more information on the flux rope modeling.

^b Scale contains semi-minor and semi-major to refer to the flatten profile. See the text for more information.

495



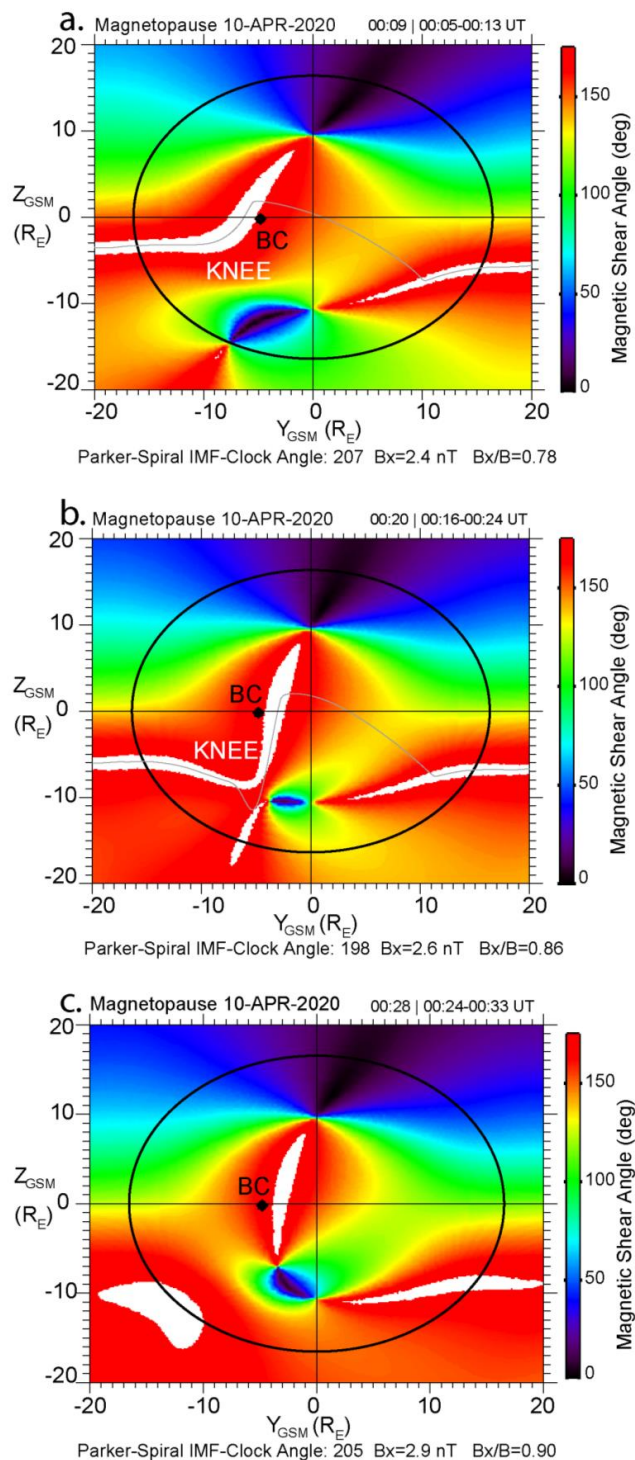
500

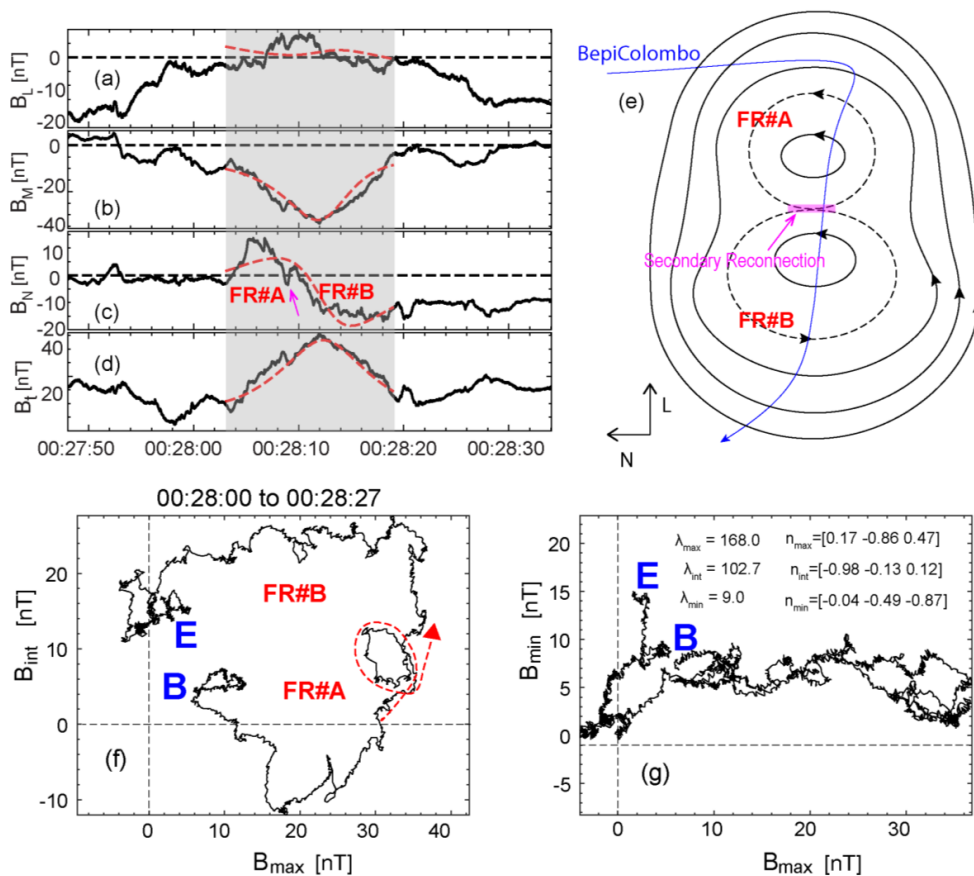
505

510

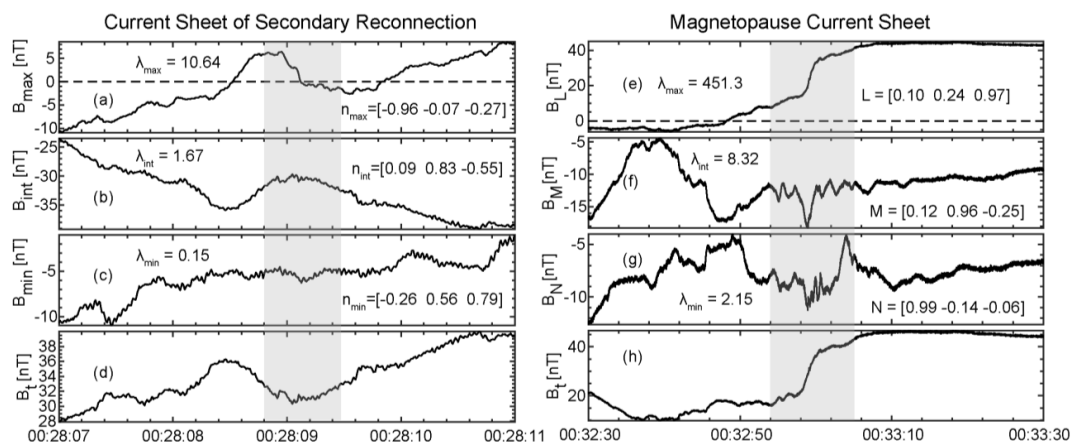
515

Figure 2. Magnetic shear angle plots on the magnetopause surface during BepiColombo’s dayside magnetopause crossing, which are obtained through the maximum magnetic shear model [Trattner et al., 2007]. (a), (b), (c) correspond to the IMF averaged from 00:05 to 00:13 UT, 00:16 to 00:24 UT and 00:24 to 00:33 UT, respectively. The black circle is the terminator plane separating the dayside magnetopause from the tailward magnetopause. The grey line is the predicted magnetopause reconnection line. White areas correspond to the magnetic shear angle is within 3° of 180° . The black dots are the location of BepiColombo (“BC”). The anti-parallel reconnection region shows a shape that is termed the “KNEE” event as it resembles a bent knee similar to an event discussed in Trattner et al. [2021].





520 **Figure 3. Overview of the flux rope centered at ~00:28:13 UT with the coalescence feature.** (a) B_L , (b) B_M , (c)
 B_N , (d) B_t . The dashed lines are obtained from the flux rope model. This LMN is the local coordinate of the
 magnetopause. See the text for more information. (e) An illustration of the coalescence event and the
 BepiColombo's trajectory. The secondary reconnection site is marked by the magenta region in (e). (f) and (g) are
 525 the hodograms of the magnetic field measurements under the local coordinate of the flux rope. The “B” and “E”
 indicate the beginning and the end of the data points. FR#A and FR#B are the two smaller flux ropes.



530 **Figure 4. The magnetic field measurements under their separately local coordinate for the reconnecting**
current sheet of the coalescence event and the magnetopause current sheet. (a) to (d) are for the coalescence
event, (e) to (h) are for the magnetopause current sheet. The eigenvalues and corresponding eigenvectors resulted
from the MVA are shown.

535